

# Detection of macrophage activity in atherosclerosis *in vivo* using multichannel, high-resolution laser scanning fluorescence microscopy

## Ashvin N. Pande

Massachusetts General Hospital  
Harvard Medical School  
Center for Molecular Imaging Research  
Charlestown, Massachusetts 02129  
and

Donald W. Reynolds Cardiovascular  
Clinical Research Center  
Harvard Medical School  
Boston, Massachusetts 02115  
and

Brigham and Women's Hospital  
Harvard Medical School  
Department of Medicine  
Cardiovascular Division  
Boston, Massachusetts 02115

## Rainer H. Kohler

Massachusetts General Hospital  
Harvard Medical School  
Center for Molecular Imaging  
Charlestown, Massachusetts 02129

## Elena Aikawa

### Ralph Weissleder

Massachusetts General Hospital  
Harvard Medical School  
Center for Molecular Imaging  
Charlestown, Massachusetts 02129  
and

Donald W. Reynolds Cardiovascular  
Clinical Research Center  
Harvard Medical School  
Boston, Massachusetts 02115

## Farouc A. Jaffer

Massachusetts General Hospital  
Harvard Medical School  
Center for Molecular Imaging  
Charlestown, Massachusetts 02129  
and

Donald W. Reynolds Cardiovascular  
Clinical Research Center  
Harvard Medical School  
Boston, Massachusetts 02115  
and

Massachusetts General Hospital  
Harvard Medical School  
Department of Medicine  
Cardiology Division  
Boston, Massachusetts 02114  
E-mail: fjaffer@partners.org

**Abstract.** Molecular and cellular mechanisms of atherogenesis and its treatment are largely being unraveled by *in vitro* techniques. We describe methodology to directly image macrophage cell activity *in vivo* in a murine model of atherosclerosis using laser scanning fluorescence microscopy (LSFM) and a macrophage-targeted, near-infrared fluorescent (NIRF) magnetofluorescent nanoparticle (MFNP). Atherosclerotic apolipoprotein E deficient (apoE  $-/-$ ) mice (n=10) are injected with MFNP or 0.9% saline, and wild-type mice (n=4) are injected with MFNP as additional controls. After 24 h, common carotid arteries are surgically exposed and prepared for LSFM. Multi-channel LSFM of MFNP-enhanced carotid atheroma ( $5 \times 5\text{-}\mu\text{m}$  in-plane resolution) shows a strong focal NIRF signal, with a plaque target-to-background ratio of  $3.9 \pm 1.8$ . Minimal NIRF signal is observed in control mice. Spectrally resolved indocyanine green (ICG) fluorescence angiograms confirm the intravascular location of atheroma. On *ex vivo* fluorescence reflectance imaging, greater NIRF plaque signal is seen in apoE  $-/-$  MFNP mice compared to controls ( $p < 0.01$ ). The NIRF signal correlates well with immunostained macrophages, both by stained surface area ( $r=0.77$ ) and macrophage number ( $r=0.86$ ). The validated experimental methodology thus establishes a platform for investigating macrophage activity in atherosclerosis *in vivo*, and has implications for the detection of clinical vulnerable plaques. © 2006 Society of Photo-Optical Instrumentation Engineers. [DOI: 10.1117/1.2186337]

**Keywords:** atherosclerosis; near-infrared fluorescence; imaging; laser scanning microscopy; macrophage; nanoparticle.

Paper 05161SSR received Jun. 30, 2005; revised manuscript received Nov. 7, 2005; accepted for publication Dec. 22, 2005; published online Mar. 23, 2006.

## 1 Introduction

Despite advances in diagnosis and treatment, atherosclerotic vascular disease remains a significant cause of morbidity and

mortality worldwide. As a result, a large effort is underway to detect high-risk, or vulnerable, atherosclerotic lesions prior to the onset of clinical events such as myocardial infarction or stroke.<sup>1</sup> Recent biological investigations have demonstrated a central role for inflammation in all phases of atherogenesis, including plaque rupture and subsequent thrombosis.<sup>2</sup> In par-

---

Address all correspondence to Farouc Jaffer, Center for Molecular Imaging Research, Massachusetts General Hospital, Harvard Medical School, MGH-CMIR — 149 13th St., Rm 5407, Charlestown, MA 02129. Tel: 617-726-5788. Fax: 617-726-5708. E-mail: fjaffer@partners.org

ticular, the macrophage has emerged as an important target for atherosclerotic therapies.<sup>3</sup> Via the generation of proinflammatory cytokines, proteolytic enzymes, and reactive oxygen species,<sup>2,3</sup> macrophages promote plaque destabilization and thus demarcate vulnerable plaques.<sup>1</sup> Functional imaging of macrophages could therefore provide further insight into their role in atherogenesis, as well as identify inflamed atheroma.

Recently, near-infrared fluorescence (NIRF) imaging of macrophage activity has been demonstrated in cancer and diabetes models *in vivo* using long-circulating magnetofluorescent nanoparticles (MFNP).<sup>4-6</sup> The dextran-coated nanoparticles are internalized by macrophages, permitting stable signal detection *in vivo*. For *in vivo* optical imaging, NIRF preparations of MFNP can be synthesized, allowing 1. relatively lower absorption of photons by endogenous molecules such as hemoglobin and water, facilitating detection of NIR photons centimeters below the surface<sup>7</sup> and 2. reduced tissue autofluorescence, allowing higher sensitivity to exogenously administered fluorochromes.<sup>8</sup> In addition, NIRF imaging can be performed with microscopic resolution *in vivo*, using methods such as epifluorescence imaging and laser scanning fluorescence microscopy (LSFM).<sup>8</sup>

In this report, we investigate the ability of dextran-coated NIRF nanoparticles (MFNP) to image macrophage activity in experimental atherosclerosis *in vivo* using LSFM, and validate these results via fluorescence reflectance imaging, fluorescence microscopy, and immunohistochemistry. The results provide a method to identify and assess macrophage activity *in vivo*, and establish a platform for investigating macrophage-related inflammation in atherosclerosis.

## 2 Methods

### 2.1 Near-Infrared Fluorescent Magnetoparticles

Briefly, a dextran-coated monodisperse iron oxide nanoparticle colloid (MION) was prepared and cross-linked with epichlorohydrin (CLIO). The mixture was then reacted with ammonia to yield NH<sub>2</sub>-functionalized cross-linked iron oxide (CLIO-NH<sub>2</sub>), as described previously.<sup>4,5</sup> A NHS-ester near-infrared fluorochrome (cyanine 5.5, excitation/emission 674/694 nm, Amersham Biosciences, United Kingdom) was subsequently conjugated to the nanoparticle by standard chemistry to produce the MFNP. The final product contained an average of 1.5 fluorochromes per nanoparticle. The mean particle size was 32 nm as determined by laser light scattering.<sup>4</sup>

### 2.2 Experimental Model of Atherosclerosis for Intravital Imaging

All animal studies were approved by the Subcommittee on Research Animal Care at Massachusetts General Hospital. Apolipoprotein E deficient (apoE<sup>-/-</sup>) mice were employed as a well-characterized experimental model of atherosclerosis.<sup>9</sup> Wild-type C57/B6 mice without atherosclerosis were included as additional controls. Female apoE<sup>-/-</sup> mice (Jackson Laboratory, Bar Harbor, Maine) were placed on an atherogenic diet (21% fat, 0.15% cholesterol, Harlan Teklad, Madison, Wisconsin) *ad libitum* beginning at 10 weeks until 32 to 36 weeks of age. Wild-type C57/B6 mice (Jackson Laboratory, Bar Harbor, Maine) were maintained on a regular diet until the time of the experiment.

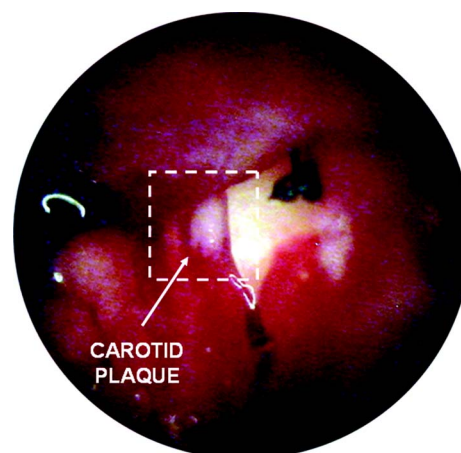


**Fig. 1** Direct surgical exposure of the right carotid artery in an apoE<sup>-/-</sup> mouse in preparation for *in vivo* laser scanning fluorescence microscopy. A typical yellowish-white atherosclerotic plaque was present at the distal common carotid artery bifurcation. A fluorescent phantom was used as reference during imaging (noted adjacent to the plaque). The dashed box represents the region displayed in laser scanning fluorescence microscopy imaged in Fig. 2(b).

For intravital imaging, MFNP was dissolved in phosphate-buffered saline and then injected via tail vein at a dose of 0.2-nmol fluorochrome/gram weight in the active (apoE<sup>-/-</sup>MFNP) group (n=7) and in the wild-type MFNP control group (n=4). Saline (0.9%) was injected in the apoE<sup>-/-</sup> saline control group (n=3). The total volume of the injection ranged between 100 and 150  $\mu$ L. After 24 h, mice were anesthetized by inhalation anesthesia (2% isoflurane, 1-L/min O<sub>2</sub>) using an isoflurane vaporizer (Bairtree Scientific, Braintree, Massachusetts). We modified a surgical model that provides access to atherosclerotic plaques in the apoE<sup>-/-</sup> mouse.<sup>10,11</sup> Briefly, the distal right common carotid artery was carefully exposed from the periadventitial tissues (Fig. 1).

Atherosclerotic plaques were visually identified and a fluorescent phantom was placed next to it as a reference during imaging. Animals were placed on a warmed glass plate and maintained on inhalation anesthesia during the one hour imaging session.

### 2.3 Laser Scanning Fluorescence Microscopy of Atherosclerotic Plaques

After isolating carotid atheroma, multichannel fluorescence imaging was performed with a prototypical laser scanning fluorescence microscope (Olympus Corporation, Japan) specifically developed for intravital near-infrared imaging of mouse organs.<sup>12</sup> Three laser lines at 488, 633, and 748 nm were used. Image acquisition was 1 s. The FluoView 300 software program (Olympus) was used to control the microscope and collect images of 512  $\times$  512 pixels with a pixel size of about 5.4  $\mu$ m/pixel and a total image size of about 2.75  $\times$  2.8 mm. Images were stored as multilayer 16-bit tagged image file format (TIFF) files. Images in the FITC channel (bandpass 505- to 525-nm filter), Cy5.5 channel (bandpass 660- to 730-nm filter), and Cy7 channel (long-pass 770-nm filter) were collected concomitantly using custom-made filters and dichroic mirrors (Olympus, Japan). A dry objective (4

× UplanApo N.A. 0.16, Olympus, Japan) with a field of view of 3.25 mm and a theoretical lateral resolution of about 2.6  $\mu\text{m}$  at 680 nm was used. Wide spectral response photo-multiplier tubes (model R928P, Hamamatsu, Japan) were used as detectors for both visible light and near-infrared signals. After initial images were obtained, a NIR vascular agent, indocyanine green (ICG), (excitation/emission 800/830 nm, Akorn, Buffalo Grove, Illinois) was administered at a dose of 5 mg/kg, and postinjection images were taken in the LSFM Cy7 channel.

The NIRF signal was determined as mean signal intensities (SI) from manually drawn regions of interest (ROI) on areas of plaque using ImageJ software (National Institutes of Health, Bethesda, Maryland). The plaque target-to-background ratio (TBR) was calculated as follows:  $\text{TBR} = [\text{SI}(\text{plaque})/\text{SI}(\text{blood})]$ .

#### 2.4 Fluorescence Reflectance Imaging

After LSFM imaging, mice were euthanized and perfused with saline and 4% paraformaldehyde. Excised carotid arteries were imaged with a custom-made NIR fluorescence reflectance imaging (FRI) system<sup>13</sup> equipped with a 150-W halogen light source and multichannel filter sets, including green fluorescent protein (GFP)/FITC (bandpass excitation 406 to 450 nm, bandpass emission 495 to 525 nm), Cy5.5 (bandpass excitation 615 to 645 nm, bandpass emission 680 to 720 nm), and ICG (bandpass excitation 716 to 756 nm, bandpass emission 780 to 820 nm) (Omega Optical, Brattleboro, Vermont). Light, Cy5.5, and GFP/FITC images were obtained (0.075, 240, and 120-s acquisitions, respectively) with a 12-bit charge-coupled device camera (Kodak, Rochester, New York) equipped with a special C-mount lens. The NIRF signal was determined as mean signal intensities from manually drawn ROI. The plaque TBR was calculated as follows:  $\text{TBR} = [\text{SI}(\text{plaque})/\text{SI}(\text{normal vessel})]$ . Epifluorescence microscopic images of resected carotid plaques were obtained with an upright fluorescence microscope (Eclipse 80i, Nikon Instruments, Melville, New York) with a cooled charge-coupled device camera (Cascade 512B, Photometrics, Tucson, Arizona).

#### 2.5 Immunohistochemistry and Fluorescence Microscopy

Excised tissues were embedded in optimal cutting temperature (OCT) compound (Tissue Tek, Sakura Finetek, Japan) and frozen in chilled isopentane. Five micrometer sections were cut from the carotid artery specimens, and fluorescence microscopy was performed in multiple channels using an upright Nikon Eclipse 80i mentioned before (FITC filter 480 $\pm$ 20 nm ex/535 $\pm$ 25 nm em/Q505LP bs; Cy5.5 filter 650 $\pm$ 22.5 nm ex/710 $\pm$ 25 nm em/Q680LP bs; ICG filter 775 $\pm$ 25 nm ex / 845 $\pm$ 27.5 nm em/ Q810LP bs). Exposure times ranged between 50 ms to 2 s. Images were analyzed with IPLab Spectrum software (Version 3.9.3, Scanalytics, Virginia). The exact same sections were then immunostained to identify macrophages within the plaque using a Mac-3 primary antibody (BD Biosciences, San Jose, California) and biotinylated secondary antibody and Vectastain ABC reagent (Vector Labs, Burlingame, California). The reaction was visualized with 3-amino-9-ethyl carbazol as substrate (AEC,

Sigma Chemical, Saint Louis, Missouri), yielding red reaction product in the cytoplasm. Nuclei were counterstained with Mayer's hematoxylin solution (Sigma Chemical). Adjacent sections were stained with hematoxylin and eosin for general morphology.

#### 2.6 Image Analysis

Digitized immunohistochemistry and fluorescence microscopy images were analyzed using IPLab Spectrum software. For quantitative image analysis, ten plaque sections were imaged with fluorescence microscopy. All images were then identically segmented by thresholding grayscale intensity at a fixed level (1750 arbitrary fluorescence units, chosen based on the average signal intensity across all images). Pixels with signal intensity above this threshold were counted as positive and summed for each section. The percent NIRF positive surface area per vessel section was calculated as follows:  $\text{NIRF}_{\text{pos}} \text{ SA}(\%) = 100\% * \frac{\sum (\text{pixels above threshold in the section})}{\sum (\text{total pixels in the section})}$ . The same sections were subsequently immunostained for macrophages (as described before) and then digitized and identically segmented by thresholding red intensity at a fixed level (88 arbitrary units, chosen based on the average signal intensity across all images) for all images. Pixels with signal intensity above this threshold were counted as positive. The percent Mac-3 positive surface area per vessel section [ $\text{Mac-3}_{\text{pos}} \text{ SA}(\%)$ ] was calculated in a similar fashion as  $\text{NIRF}_{\text{pos}} \text{ SA}(\%)$ . For further analysis, 12 representative regions of interest (1000 pixel uniform area) in four plaque sections of varying macrophage content were randomly selected, and the average NIRF signal intensity in each ROI (in arbitrary fluorescence units) was measured using IPLab Spectrum software. The number of cells expressing a Mac-3 antigen (defined as a red reaction product associated with a blue hematoxylin nuclear counterstain) was then counted by an experienced pathologist (EA) in ten high-power fields for each corresponding ROI region using an eyepiece reticle (10 mm, 1-mm division; Fisher Scientific) and correlated with the average NIRF signal intensity of the same ROI.

#### 2.7 Statistical Methods

All results are reported as mean $\pm$ SD. For differences between multiple groups, a one-way ANOVA followed by a *post-hoc* Tukey's test for multiple comparisons was used. All statistics including linear regressions were performed using GraphPad Prism version 4.03 for Windows (GraphPad Software, San Diego, California). A p-value of <0.05 was considered significant.

### 3 Results

#### 3.1 Laser Scanning Fluorescence Microscopy Identifies Magnetofluorescent Nanoparticles in Carotid Atheroma

Discrete right common carotid atherosclerotic lesions were visually identified *in situ* (Fig. 1) and imaged *in vivo* in all apoE *-/-* animals (n=10, Fig. 1); lesions were not present in any of the four wild-type animals. In apoE *-/-* animals injected with MFNP, the LSFM images showed focal areas of NIRF signal in carotid atheroma, consistent with MFNP uptake [Fig.

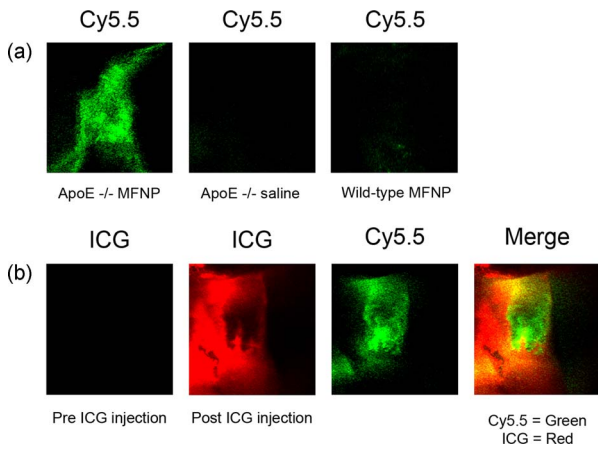


**Fig. 2** (a) Representative intravital laser scanning fluorescence microscopy Cy5.5 channel images from an apoE <sup>-/-</sup> MFNP-injected animal, an apoE <sup>-/-</sup> saline control, and a wild-type MFNP control. Strong NIRF signal in plaques was evident in apoE <sup>-/-</sup> MFNP-injected animals but not in controls. The Cy5.5 channel NIRF images were windowed identically. (b) Additional intravital laser scanning fluorescence microscopy images from a different apoE <sup>-/-</sup> MFNP-injected mouse also revealed bright, focal Cy5.5 signal in plaque. Signal in the ICG channel prior to indocyanine green injection was minimal at baseline. Subsequent ICG injection provided a definition of the vascular space and revealed an intravascular filling defect, further confirming the location of plaques detected in the MFNP channel.

2(a)]. In comparison, there was minimal NIRF signal in the apoE <sup>-/-</sup> saline control group [Fig. 2(a)] consistent with low autofluorescence in the NIR window.<sup>8</sup> A relatively low level of intravascular NIRF signal was also seen, likely from residual circulating MFNP. In addition, no significant vascular wall NIRF signal was seen in the wild-type MFNP group, consistent with the absence of atherosclerosis. Subsequent injection of a vascular agent, indocyanine green (ICG), defined the arterial lumen and visualized plaques as angiographic filling defects [Fig. 2(b)] The target-to-background ratio between the plaque and the adjacent blood (TBR) in the Cy5.5 channel in the apoE <sup>-/-</sup> MFNP group was 3.9 ± 1.8.

### 3.2 Ex-vivo Near-Infrared Fluorescence Imaging Confirms Magnetofluorescent Nanoparticle Localization in Plaque

Fluorescence reflectance images and epifluorescence microscopic images of excised carotid atheromata were obtained to corroborate the LSFM findings. The images showed focal NIRF signal in plaque, with minimal NIRF signal in the normal arterial wall [Fig. 3(a)]. The plaque target-to-background ratio was 4.8 ± 1.8 in the MFNP-injected group, 1.3 ± 0.2 in the saline-injected group, and 1.1 ± 0.1 in the wild-type group (p < 0.01 ANOVA):[Fig. 3(b)]

### 3.3 Atherosclerotic Plaque Near-Infrared Fluorescence Signal Colocalizes with Macrophages

Multiwavelength fluorescence microscopy was performed on frozen sections of carotid arteries. Fluorescence microscopy in the Cy5.5 channel showed strong signal in regions of atherosclerotic plaques [Fig. 4(a)]. The plaque NIRF signal colo-

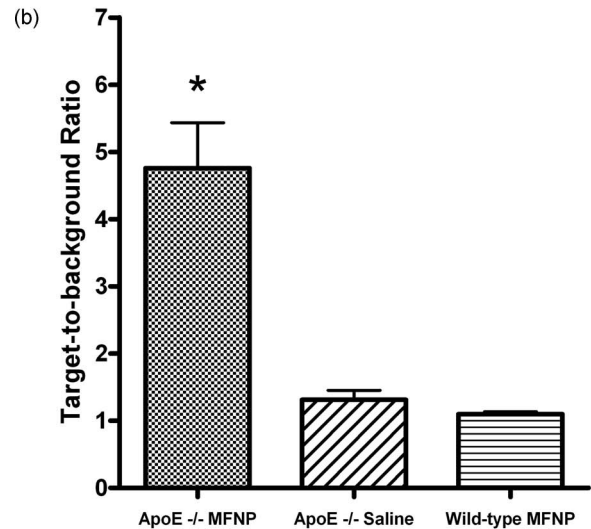
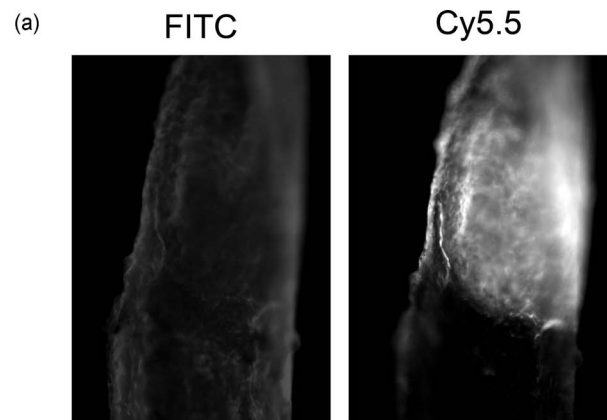


**Fig. 3** Fluorescence reflectance imaging of an excised carotid atheroma from an apoE <sup>-/-</sup> MFNP-injected animal showed bright enhancement in the Cy5.5 channel, consistent with MFNP localization in plaque and distinct from autofluorescence seen in the FITC channel. (b) The plaque TBR from apoE <sup>-/-</sup> MFNP-injected animals was significantly greater than the control groups. \*p < 0.01 versus each of the two control groups.

calized with the cellular-rich zones of plaques, typically superficial in the employed atherosclerotic model. Images in multiple fluorescence channels were obtained and confirmed that Cy5.5 signal was distinct from autofluorescence [Fig. 4(a)]. A low level of nonspecific ICG fluorescent signal was seen on the endoluminal surface of the vessels and in the periadventitial areas. Correlative immunohistochemistry confirmed that the NIRF signal colocalized with areas rich in macrophages [Fig. 4(b)], consistent with earlier studies.<sup>4,5</sup> The percent of NIRF-positive surface area per vessel section correlated with the percent of Mac-3-immunostaining-positive surface area per vessel section (r = 0.77) [Fig. 5(a)]. Furthermore, when macrophage staining was quantified as the number of cells per region of interest (ROI), the NIRF-macrophage correlation became stronger (r = 0.86) [Fig. 5(b)].

## 4 Discussion

Using a NIRF magnetofluorescent nanoparticle and intravital laser scanning fluorescence microscopy, we demonstrate that

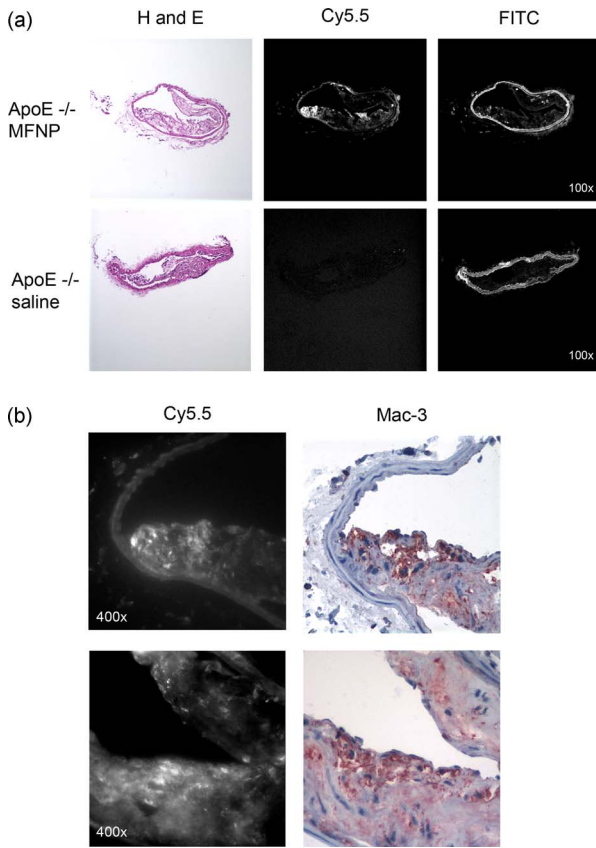


**Fig. 4** (a) Fluorescence microscopy showed focal NIRF signal in cellular-rich areas of plaques from apoE<sup>-/-</sup> MFNP-injected animals and negligible NIRF signal in control plaques. The Cy5.5 channel NIRF images were windowed identically. (b) Correlative immunohistochemistry confirmed colocalization of the NIRF signal with macrophages as detected by Mac-3 immunostaining.

macrophage activity in atherosclerosis can be imaged at microscopic resolutions *in vivo*. ApoE<sup>-/-</sup> mice injected with the MFNP demonstrated high plaque target-to-background ratios and focal NIRF signal within carotid atheroma. Minimal autofluorescent NIRF signal was evident in saline-injected apoE<sup>-/-</sup> mice or in MFNP-injected wild-type mice. Similar results were seen on *ex vivo*. FRI of carotid plaques, revealed a 369% increase in the plaque-vessel TBR compared to saline-injected apoE<sup>-/-</sup> mice. On correlative histopathology and fluorescence microscopy, we found strong focal NIRF signal in MFNP-enhanced atheroma, primarily in the cellular-rich zones of lesions. A good correlation was found between the plaque NIRF signal and immunostained plaque macrophages. These results validate this approach for imaging macrophage activity at microscopic resolutions *in vivo* using MFNP-enhanced laser scanning fluorescence microscopy.

Macrophages are involved in all phases of atherogenesis including plaque rupture, and their presence is felt to identify high-risk, vulnerable atherosclerotic plaques.<sup>1,2</sup> Consequently, a number of molecular imaging strategies have been developed for detecting macrophage activity in atherosclerosis (reviewed in Ref. 14). In this investigation, we employed a long-circulating, macrophage-avid, prototype NIRF nanoparticle (MFNP) to detect macrophage activity *in vivo*. Macrophage

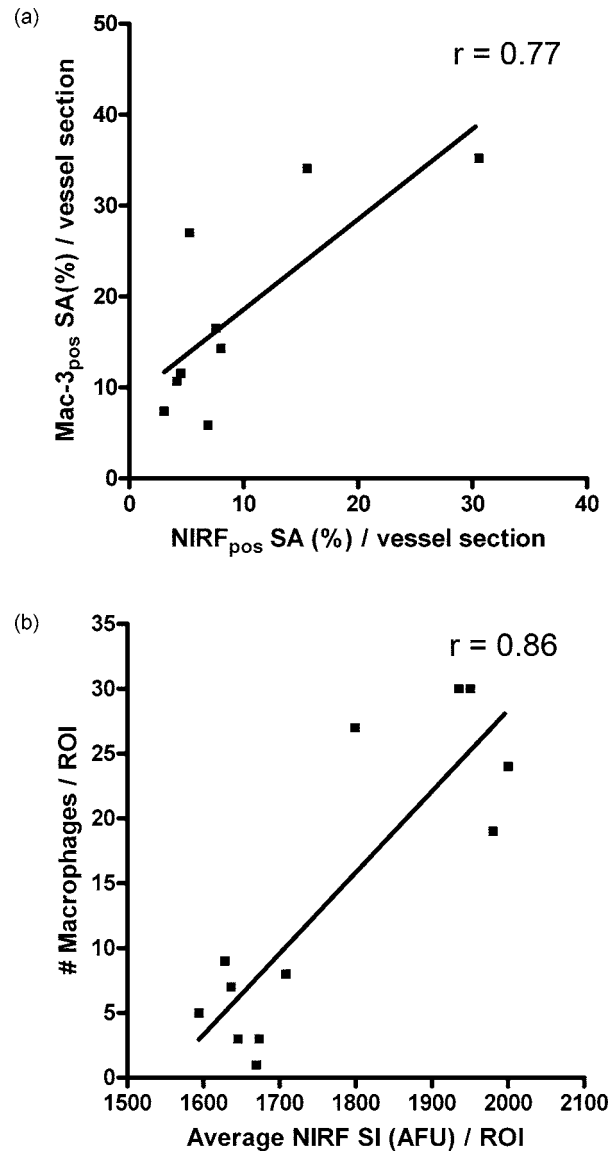


**Fig. 5** (a) Quantitative histological analysis showed a strong correlation between the percent NIRF-positive plaque signal [NIRF<sub>pos</sub> SA(%)] and the macrophage Mac-3 immunostained surface area [Mac-3<sub>pos</sub>SA(%)] ( $r=0.77$ ). (b) Furthermore, the average NIRF signal intensity per ROI also correlated strongly with the number of macrophages per ROI ( $r=0.86$ ). SI=signal intensity, AFU=arbitrary fluorescence units.

uptakes of these nanoparticles have been demonstrated in both experimental and clinical studies,<sup>4,5,15-18</sup> and increases *in vitro* with inflammatory stimuli.<sup>19</sup> Mechanistically, uptake of these nanoparticles is thought to occur by fluid phase endocytosis.<sup>20</sup> Additional internalization via the macrophage scavenger receptor A (SR-A)<sup>21</sup> or via a specific receptor for oligosaccharides such as dextran<sup>6</sup> may also contribute to the uptake of MFNP by macrophages.

The current experimental and imaging system offers several advantages for imaging macrophage activity in atherosclerosis. First, multichannel laser scanning fluorescence microscopy allows high-resolution imaging of plaque structures. The current in-plane resolution of  $5 \times 5 \mu\text{m}$  approaches the

ability to resolve single macrophages (~10 to 30 microns in diameter) *in vivo*. This level of resolution offers the potential for studying cell trafficking and dynamic studies of inflammation within atheroma. In addition, the availability of multiple optical channels helps to resolve distinct anatomical spaces (e.g., vessel lumen, plaque, etc.) and affords optimal structural definition. Furthermore, imaging in the near-infrared window allows reasonable tissue depth penetration and reduced autofluorescence in this carotid atheroma model, as witnessed by the observed high plaque target-to-background ratio. Potential biological extensions of this study could include assessing atherosclerosis therapies such as HMG-CoA reductase inhibitors ("statins"), as well as studying the interaction of fluorescently labeled blood cells (e.g., platelets, leukocytes) with MFNP-labeled plaque nanoparticles.<sup>10,11</sup>

From a clinical perspective, imaging of the inflammatory process in atherosclerosis offers the ability to identify vulnerable plaques.<sup>1</sup> Although the current imaging approach is surgically invasive and the clinical translation of the described methodology would pose many challenges, the development of minimally invasive intravascular NIRF imaging catheters holds promise as an alternative to image NIR fluorescent atherosclerotic plaques *in vivo*.<sup>22</sup> Furthermore, catheter-based NIRF imaging can be integrated with optical coherence tomography (OCT)<sup>23</sup> to further image atherosclerotic plaque components,<sup>24,25</sup> as well as macrophage content in atherosclerotic lesions.<sup>26</sup> A combined NIRF-OCT catheter could therefore allow both functional and structural identification of plaque macrophages, allowing a more comprehensive study of vulnerable plaques. From an imaging agent perspective, MRI of dextran-coated magnetic nanoparticles has been performed clinically to detect inflammation in atherosclerosis at lower (millimeter) resolution.<sup>27</sup> Another potential advantage of MFNP, although beyond the scope of the present study, could be to couple noninvasive MRI with intravital LSFM to provide complementary, multimodal images of inflammation in atherosclerosis. The presently employed MFNP therefore represents a next-generation nanoparticle that could eventually allow clinical NIRF imaging of macrophage activity in patients. Ultimately, assessment of inflammation in atheroma may ultimately allow better identification, risk stratification, and treatment of vulnerable plaques.

There are limitations to our study. Higher magnification objectives were also available on the LSFM system, but were not employed in this model due to motion artifact. Other models or additional vessel stabilizing techniques could reduce motion artifact, allowing higher resolution LSFM. Obtaining high-quality vascular angiograms was limited by the extravasation of indocyanine green into the surrounding tissue. The alternative use of long-circulating intravascular fluorescent imaging agents could overcome this limitation.<sup>28</sup> Although the majority of the MFNP localized in macrophages in atheroma, endothelial cells, and smooth muscle cells were occasionally noted to contain the nanoparticles, consistent with prior studies of dextran-coated nanoparticles.<sup>17</sup> As mentioned earlier, the surgically invasive imaging approach has limited clinical applicability, though the development of minimally invasive intravascular NIRF imaging catheters<sup>22</sup> and noninvasive fluorescence imaging systems<sup>7</sup> may offer clinically viable imaging options in the future.

In conclusion, we demonstrate high-resolution, *in vivo*

near-infrared fluorescence imaging of macrophage activity in atherosclerosis. This validated imaging platform employs a macrophage-targeted magnetofluorescent nanoparticle that can be readily detected by laser scanning fluorescence microscopy. This approach offers a high-resolution platform for imaging inflammation in atherosclerosis *in vivo*, and should prove useful for assessing perturbations of macrophage biology.

### Acknowledgments

Donald W. Reynolds Foundation (Pande, Aikawa, Weissleder, and Jaffer) National Institutes of Health P50-CA86355, (Weissleder), and R24-CA92782 (Weissleder). Pande is a Donald W. Reynolds Cardiovascular Research Fellow. The authors acknowledge the CMIR Mouse Imaging Program team (Umar Mahmood, Ralph Weissleder, Herlen Alencar, and Pratik Patel) and Yoshihiro Kawano and Tadashi Hirata of the Olympus Corporation, Japan, for extensive development and validation work of the NIR laser scanning fluorescent microscopy. We also acknowledge Nikolai Sergeev for synthesis of the MFNP agent, and Karen Mendelson for technical assistance.

### References

1. M. Naghavi, P. Libby, E. Falk, S. W. Casscells, S. Litovsky, J. Rumberger, J. J. Badimon, C. Stefanadis, P. Moreno, G. Pasterkamp, Z. Fayad, P. H. Stone, S. Waxman, P. Raggi, M. Madjid, A. Zarrabi, A. Burke, C. Yuan, P. J. Fitzgerald, D. S. Siscovick, C. L. de Korte, M. Aikawa, K. E. Juhani Airaksinen, G. Assmann, C. R. Becker, J. H. Chesebro, A. Farb, Z. S. Galis, C. Jackson, I. K. Jang, W. Koenig, R. A. Lodder, K. March, J. Demirovic, M. Navab, S. G. Priori, M. D. Reikher, R. Bahr, S. M. Grundy, R. Mehran, A. Colombo, E. Boerwinkle, C. Ballantyne, W. Insull Jr., R. S. Schwartz, R. Vogel, P. W. Serruys, G. K. Hansson, D. P. Faxon, S. Kaul, H. Drexler, P. Greenland, J. E. Muller, R. Virmani, P. M. Ridker, D. P. Zipes, P. K. Shah, and J. T. Willerson, "From vulnerable plaque to vulnerable patient: a call for new definitions and risk assessment strategies: Part I," *Circulation* **108**(14), 1664–1672 (2003).
2. P. Libby, "Inflammation in atherosclerosis," *Nature (London)* **420**(6917), 868–874 (2002).
3. A. C. Li and C. K. Glass, "The macrophage foam cell as a target for therapeutic intervention," *Nat. Med.* **8**(11), 1235–1242 (2002).
4. M. F. Kircher, U. Mahmood, R. S. King, R. Weissleder, and L. Josephson, "A multimodal nanoparticle for preoperative magnetic resonance imaging and intraoperative optical brain tumor delineation," *Cancer Res.* **63**(23), 8122–8125 (2003).
5. M. C. Denis, U. Mahmood, C. Benoit, D. Mathis, and R. Weissleder, "Imaging inflammation of the pancreatic islets in type 1 diabetes," *Proc. Natl. Acad. Sci. U.S.A.* **101**(34), 12634–12639 (2004).
6. K. Nagaoka, K. Takahara, K. Tanaka, H. Yoshida, R. M. Steinman, S. Saitoh, S. Akashi-Takamura, K. Miyake, Y. S. Kang, C. G. Park, and K. K. Inaba, "Association of SIGNR1 with TLR4-MD-2 enhances signal transduction by recognition of LPS in gram-negative bacteria," *Int. Immunol.* **17**(7), 827–836 (2005).
7. V. Ntziachristos, J. Ripoll, and R. Weissleder, "Would near-infrared fluorescence signals propagate through large human organs for clinical studies?," *Opt. Lett.* **27**(5), 333–335 (2002).
8. R. Weissleder and V. Ntziachristos, "Shedding light onto live molecular targets," *Nat. Med.* **9**(1), 123–128 (2003).
9. K. S. Meir and E. Leitersdorf, "Atherosclerosis in the apolipoprotein-E-deficient mouse: a decade of progress," *Arterioscler., Thromb., Vasc. Biol.* **24**(6), 1006–1014 (2004).
10. E. E. Eriksson, X. Xie, J. Werr, P. Thoren, and L. Lindbom, "Direct viewing of atherosclerosis *in vivo*: plaque invasion by leukocytes is initiated by the endothelial selectins," *FASEB J.* **15**(7), 1149–1157 (2001).
11. Y. Huo, A. Schober, S. B. Forlow, D. F. Smith, M. C. Hyman, S. Jung, D. R. Littman, C. Weber, and K. Ley, "Circulating activated platelets exacerbate atherosclerosis in mice deficient in apolipoprotein E," *Arterioscler., Thromb., Vasc. Biol.* **24**(6), 1006–1014 (2004).

- tein E," *Nat. Med.* **9**(1), 61–67 (2003).
12. H. Alencar, U. Mahmood, Y. Kawano, T. Hirata, and R. Weissleder, "Novel multiwavelength microscopic scanner for mouse imaging," *Neoplasia* **7**(11), 977–983 (2005).
  13. U. Mahmood, C. H. Tung, Y. Tang, and R. Weissleder, "Feasibility of *in vivo* multichannel optical imaging of gene expression: experimental study in mice," *Radiology* **224**(2), 446–451 (2002).
  14. F. A. Jaffer and R. Weissleder, "Seeing within: molecular imaging of the cardiovascular system," *Circ. Res.* **94**(4), 433–445 (2004).
  15. S. A. Schmitz, S. E. Coupland, R. Gust, S. Winterhalter, S. Wagner, M. Kresse, W. Semmler, and K. J. Wolf, "Superparamagnetic iron oxide-enhanced MRI of atherosclerotic plaques in Watanabe heritable hyperlipidemic rabbits," *Invest. Radiol.* **35**(8), 460–471 (2000).
  16. S. G. Ruehm, C. Corot, P. Vogt, S. Kolb, and J. F. Debatin, "Magnetic resonance imaging of atherosclerotic plaque with ultrasmall superparamagnetic particles of iron oxide in hyperlipidemic rabbits," *Circulation* **103**(3), 415–422 (2001).
  17. M. E. Kooi, V. C. Cappendijk, K. B. Cleutjens, A. G. Kessels, P. J. Kitslaar, M. Borgers, P. M. Frederik, M. J. Daemen, and J. M. van Engelshoven, "Accumulation of ultrasmall superparamagnetic particles of iron oxide in human atherosclerotic plaques can be detected by *in vivo* magnetic resonance imaging," *Circulation* **107**(19), 2453–2458 (2003).
  18. R. A. Trivedi, U. K. I. JM, M. J. Graves, J. J. Cross, J. Horsley, M. J. Goddard, J. N. Skepper, G. Quartey, E. Warburton, I. Joubert, L. Wang, P. J. Kirkpatrick, J. Brown, and J. H. Gillard, "In vivo detection of macrophages in human carotid atheroma: temporal dependence of ultrasmall superparamagnetic particles of iron oxide-enhanced MRI," *Stroke* **35**(7), 1631–1635 (2004).
  19. W. J. Rogers and P. Basu, "Factors regulating macrophage endocytosis of nanoparticles: implications for targeted magnetic resonance plaque imaging," *Atherosclerosis* **178**(1), 67–73 (2005).
  20. R. Weissleder, K. Kelly, E. Y. Sun, T. Shtatland, and L. Josephson, "Cell-specific targeting of nanoparticles by multivalent attachment of small molecules," *Nat. Biotechnol.* **23**(11), 1418–1423 (2005).
  21. I. Raynal, P. Prigent, S. Peyramaure, A. Najid, C. Rebutzi, and C. Corot, "Macrophage endocytosis of superparamagnetic iron oxide nanoparticles: mechanisms and comparison of ferumoxides and ferumoxtran-10," *Invest. Radiol.* **39**(1), 56–63 (2004).
  22. B. Zhu, F. A. Jaffer, V. Ntziachristos, and R. Weissleder, "Development of a near infrared fluorescence catheter: operating characteristics and feasibility for atherosclerotic plaque detection," *J. Phys. D* **38**, 1–7 (2005).
  23. J. K. Barton, F. Guzman, and A. Tumlinson, "Dual modality instrument for simultaneous optical coherence tomography and fluorescence spectroscopy," *J. Biomed. Opt.* **9**(3), 618–623 (2004).
  24. H. Yabushita, B. E. Bouma, S. L. Houser, H. T. Aretz, I. K. Jang, K. H. Schlendorf, C. R. Kauffman, M. Shishkov, D. H. Kang, E. F. Halpern, and G. J. Tearney, "Characterization of human atherosclerosis by optical coherence tomography," *Circulation* **106**(13), 1640–1645 (2002).
  25. I. K. Jang, B. E. Bouma, D. H. Kang, S. J. Park, S. W. Park, K. B. Seung, K. B. Choi, M. Shishkov, K. Schlendorf, E. Pomerantsev, S. L. Houser, H. T. Aretz, and G. J. Tearney, "Visualization of coronary atherosclerotic plaques in patients using optical coherence tomography: comparison with intravascular ultrasound," *J. Am. Coll. Cardiol.* **39**(4), 604–509 (2002).
  26. G. J. Tearney, H. Yabushita, S. L. Houser, H. T. Aretz, I. K. Jang, K. H. Schlendorf, C. R. Kauffman, M. Shishkov, E. F. Halpern, and B. E. Bouma, "Quantification of macrophage content in atherosclerotic plaques by optical coherence tomography," *Circulation* **107**(1), 113–119 (2003).
  27. F. A. Jaffer and R. Weissleder, "Molecular imaging in the clinical arena," *JAMA, J. Am. Med. Assoc.* **293**(7), 855–862 (2005).
  28. L. Josephson, U. Mahmood, P. Wunderbaldinger, Y. Tang, and R. Weissleder, "Pan and sentinel lymph node visualization using a near-infrared fluorescent probe," *Molecular Imaging* **2**(1), 18–23 (2003).